Crystallization and impact history of a meteoritic sample of early lunar crust (NWA 3163) refined by atom probe geochronology

White, L. F.[1,2*], Moser, D. E.[3], Tait, K. T.[1,2], Langelier, B.[4], Barker, I.[3] & Darling, J. R.[5]

[1]*Centre for Applied Planetary Mineralogy, Department of Natural History, Royal Ontario Museum, Toronto, Ontario, M5S 2C6, Canada*

[2]*Department of Earth Sciences, University of Toronto, Toronto, Ontario, M5S 3B1, Canada*

[3]*Department of Earth Sciences, University of Western Ontario, London, N6A 5B7, Canada.*

[4]*Canadian Centre for Electron Microscopy, McMaster University, Hamilton, Ontario, Canada*

[5]*School of Earth and Environmental Science, University of Portsmouth, Portsmouth, UK.*

**Corresponding Author; lwhite@rom.on.ca*

Key Words: Baddeleyite; U-Th-Pb isotopes; EBSD; Atom Probe Tomography; Geochronology; Northwest Africa 3163

Granulitic lunar meteorites offer rare insights into the timing and nature of igneous, metamorphic and impact processes in the lunar crust. Accurately dating the different events recorded by these materials is very challenging, however, due to low trace element abundances (e.g. Sm, Nd, Lu, Hf), micrometer-scale U-Th-bearing accessory minerals, and disturbed Ar-Ar systematics following a multi-stage history of shock and thermal metamorphism. Here we report on micro-baddeleyite grains in granulitic mafic breccia NWA 3163 for the first time and show that targeted microstructural analysis (electron backscatter diffraction) and nanoscale geochronology (atom probe tomography) can overcome these barriers to lunar chronology. A twinned (~90°/<401>) baddeleyite domain yields a $^{232}Th/^{208}Pb$ age of 4328 ± 309 Ma, which overlaps with a robust secondary ion mass spectrometry (SIMS) $^{207}Pb/^{206}Pb$ age of 4308 ± 18.6 Ma and is interpreted here as the crystallization age for an NWA 3163 protolith. A second microstructural domain, < 2µm in width, contains patchy overprinting baddeleyite and yields a Th-Pb age of 2175 ± 143 Ma, interpreted as dating the last substantial impact event to affect the sample. This finding demonstrates the potential of combining microstructural characterization with nanoscale geochronology when resolving complex *P-T-t* histories in planetary materials, here yielding the oldest measured crystallization age for components of lunar granulite NWA 3163 and placing further constraints on the formation and evolution of lunar crust.

1. Introduction

Northwest Africa (NWA) 3163, along with paired stones NWA 4881 and NWA 4483, potentially represents the largest sample of granulitic lunar crust available for study (i.e. Hudgins et al., 2011). These stones appear to represent a region of the Moon that has not been directly sampled by either the Apollo or Luna missions, facilitating a more global appraisal of lunar crustal processes (Hudgins et al., 2011; McLeod et al. 2016). Generating accurate, precise and robust ages for specific events recorded within these samples is paramount to testing contrasting models for the formation, differentiation and bombardment history of the Moon, such as whether there was a global lunar magma ocean (Borg et al., 2011) and, later, a period of intense impact bombardment known as the lunar cataclysm at ~3.9 Ga (Cohen et al., 2000). Such efforts are further complicated in meteoritic samples by additional deformation induced during shock loading and ejection from the lunar surface (i.e. Joy and Arai, 2013), which can overprint mineralogical evidence of both crystallization and earlier, more severe impact events that cumulatively result in bombardment. More recently, dating of microstructurally characterised accessory phases, such as titanite (Papapavlou et al., 2018) and monazite (Erickson et al., 2017), have proven to be useful impact chronometers, though these phases are less widespread in planetary (lunar, martian, asteroidal) lithologies. Robust Zr-bearing phases, such as zircon ($ZrSiO_4$) and baddeleyite (ZrO_2), have proven to be ideal U-Th-Pb chronometers in such materials, often preserving a spread of ages between crystallization and bombardment despite extensive overprinting by younger deformation (Moser et al., 2013; Cavosie et al., 2015; Darling et al., 2016). Baddeleyite is particularly promising as a planetary chronometer given the wide-spread occurrence of the phase within the mafic rocks that dominate the Solar System (Herd et al., 2018) and the exclusion of common Pb during crystallization (Heaman and LeCheminant, 1993). However, discrete domains with varying U-Th-Pb ages may often be preserved on the micrometre to sub nanometre scale in highly shocked zircon and baddeleyite (Moser et al., 2011; Cavosie et al., 2015; White et al., 2017a). These can be unravelled by coupling techniques such as electron backscatter diffraction (EBSD; Cavosie et al. 2015; Darling et al. 2016; White et al. 2018), secondary ionisation mass spectrometry (SIMS; Moser et al., 2013) and atom probe tomography (APT; White et al., 2017a; White et al., 2017b) to generate structurally characterised ages. Here we analyse baddeleyite grains in a unique piece of the deep lunar crust (NWA 3163; Irving et al., 2006) to yield an accurate age for both crystallization and shock loading of the sample. Despite major efforts with the Sr and Ar isotopic systems (McLeod et al., 2016; Hudgins et al., 2011; Fernandes et al., 2009), very broad chronological brackets have so far been interpreted for the evolution of NWA 3163. Our goal is to further refine this chronology with attention to the mineral crystallization (as opposed to mantle separation) age and timing of granularization in such challenging samples using minimally destructive techniques as a contribution to lunar and meteorite chronology.

2. Material and Methods

Lunar meteorite NWA 3163 is a breccia composed of centimeter-sized gabbroic and gabbro-anorthositic clasts within a finer grained matrix exhibiting a granulitic texture cross-cut by later shock veining (**Figure 1**). Chemically, the breccia plots as part of the ferroan anorthosite suite (FAS), suggesting its lithic components can be traced to an early lunar crust which formed directly from remelting and recrystallization of differentiated lunar magma ocean products (McLeod et al., 2016). The sample contains pervasive maskelynite (diaplectic glass of plagioclase composition) which, given the composition of the feldspar (An_{94}), is suggestive of shock pressures in excess of 20 – 24 GPa (Fritz et al., 2011). Mantle separation of parental magma for the breccia components is placed at 4340 ± 57 Ma based on a source model Sr T_{RD} age (McLeod et al. 2016). Uniformity of Sr and trace element composition among components suggests derivation from a single source of early (~4300 Ma) lunar crust of the FAS (McLeod et al. 2016). Ar-Ar geochronology yields ages of ~3350 Ma (McLeod et al. 2016) and ~1980 Ma (Hudgins et al. 2011), which are attributed to granularization of the sample and a younger shock event, respectively.

Target baddeleyite grains were located and imaged in three thin sections of NWA 3163 using a combination of automated backscatter electron (BSE) and energy-dispersive X-ray spectroscopy (EDS) techniques using the Oxford Instruments INCA 'Feature' modules and Oxford X-Max 80 detector installed on electron microscopes at the Zircon and Accessory Phase Laboratory (ZAPlab) at the University of Western Ontario, Canada. Target grains were imaged using BSE and secondary electron (SE) techniques, and micro- to nano-scale structural analysis was conducted by electron backscatter diffraction (EBSD) using an Oxford Instruments Nordlys EBSD detector mounted on a Hitachi SU6600 field emission gun SEM (FEG-SEM; ZAPLab) following previously reported analytical conditions (i.e. Darling et al., 2016). Generated baddeleyite diffraction patterns were matched to inorganic crystal structure database (ICSD) card 15,983 using crystal lattice parameters of a = 5.21, b = 5.26, c = 5.37, and α = 90°, β = 80.5°, γ = 90° (Smith & Newkirk 1965). Wild spike reduction was completed on all EBSD datasets, although no other form of raw data correction was conducted.

Within a separate mount, secondary ion mass spectrometry (SIMS) analysis of U-Th-Pb systematics was conducted on three grains following previously reported procedure (Schmitt et al., 2010; Moser et al., 2013; Darling et al., 2016). Correlative EBSD work was not conducted on these grains prior to analysis.

Grain #12,112 was selected for detailed atom probe tomography (APT) analysis following EBSD characterisation. The grain was extracted using a Zeiss NVision 40 SEM hosted by the Canadian Centre for Electron Microscopy (CCEM) at McMaster University, Canada, using a focused Ga ion beam (FIB) operating at 30 kV and 13 nA. A 10 kV 80 pA beam was used for final sharpening to minimize any potential damage or Ga ion implantation. The lift out of the grain was subsampled to yield five microtip specimens for APT analysis. Microtips were analysed using a CAMECA local electrode atom probe (LEAP) 4000X HR instrument housed at CCEM, following analytical procedures outlined by previous baddeleyite APT studies (White et al., 2017a; White et al., 2017b), operating the 355nm wavelength laser at 100 pJ and 125 kHz, with a targeted detection rate of 3%. Mass-to-charge peaks were background corrected using the IVAS software package using a local range assisted estimate of the background. Isotopic uncertainties are calculated by propagating counting statistics errors of the individual background corrected peaks through to the final isotopic ratio. Full details regarding APT instrument settings, data reduction and reconstruction can be found in the supplementary materials, reported following the recommendations of Blum et al. 2018.

3. Results

3.1 Correlative imaging, microscopy and chronology of baddeleyite

SEM scans of three thin sections of NWA 3163 reveal a total of nine baddeleyite grains. These grains are generally < 10μm in the longest dimension, occurring primarily in association with ilmenite (~90%) and rarely with flow-textured feldspathic melt veins. Most grains appear homogenous in backscatter electron imaging, with no visible fractures or surface defects of note, though one of the examined baddeleyite contains cross-cutting, open fractures which we ascribe to the ejection event (**Figure 2**). EBSD analysis of four grains reveals a range of complex microstructures, including polysynthetic twinning, patchy baddeleyite domains with small (sub-micrometre) granules, and domains of poorly diffracting ZrO_2 (**Figure 3**). Two grains completely enclosed in highly fractured ilmenite contain larger subdomains of crystal plastically deformed (< 10°) baddeleyite of a single orientation (**Figure 3b,d**), though this deformation is largely controlled by fracturing and associated deformation within the crystals. Within directional pole figures for baddeleyite, clusters of orthogonally related (90°) crystallographic orientations can be observed, though these do not demonstrate the localised ~18° crosses associated with reversion from high pressure and temperature ZrO_2 phases (Timms et al., 2017; White et al., 2018).

SIMS analysis was attempted on three grains in a separate mount, though only a single analysis yielded a high amount of radiogenic Pb (98%). The two analyses with low percentages of radiogenic Pb (40 and 19% respectively) are ascribed to difficulty in targeting these single micron scale grains during SIMS analysis. The successfully targeted baddeleyite crystal yields a $^{207}Pb/^{206}Pb$ age of 4308 ± 37 Ma (2σ) and has U-Pb systematics that are concordant, albeit with relatively large uncertainties on U-Pb ratios. All SIMS data are reported in the supplementary materials.

During extraction of the atom probe microtips, the target baddeleyite grain (#12,112) was imaged prior to lift out. This reveals that large fractures in the surrounding ilmenite phase form a complex structural network surrounding the baddeleyite, though these features terminate at the baddeleyite grain boundary (**Figure 4a,b**). In addition, the baddeleyite itself contains minor nanoscale fractures, though appears relatively undeformed compared to the surrounding mineral assemblage. EBSD analysis of the grain reveals similar microstructural features to those observed in all other grains, principally subdomains of degraded crystallinity (**Figure 4c**) and complex crystalline subdomains. The surrounding ilmenite (**Figure 4d**) is highly crystalline, preserving undeformed lamellae twins which record $180°/<\bar{2}110$ relationships. The baddeleyite grain contains two distinct subdomains, with polysynthetic twins yielding ~90°/<401> orientation relationships, and a patchy baddeleyite domain which is consistently misorientated ~120°/< relative to the primary orientations (**Figure 4e**). In isolation, only the twinned domain hosts orthogonal relationships, while the patchy domains (purple data points in **Figure 4f**) contain no obvious microstructural complexity.

3.2 Nanostructural geochronology by atom probe tomography (APT)

Of the five prepared microtip specimens, two produced reliable (< 20 ppm/ns background) APT datasets in excess of 38.6 (#01665) and 112 (#01667) million collected ions. These tips were extracted from microstructurally distinct domains of the target baddeleyite grain (grey and white stars in **Figure 4e**), with microtip #01665 representing the patchy domain and microtip #01667 sampling the polysynthetically twinned central domain. The tips are chemically similar, yielding ~99 atomic percent (at%) Zr and O cations and molecular species, predominately evaporated as ZrO and ZrO_2. Trace element impurities are quantified in both microtips, with the most prominent contaminants (Hf, Ti, Nb, P) being measured to within ± ~1% 2σ certainty due to the large amount of ionic counts. Other species (Mg, Al, La, Ce, Mn) yield minimal counts and fall below the detection threshold of APT, particularly in the smaller dataset (**Supplementary Materials**). Fe/Si ratios are comparable in both tips (~8). All atoms and compounds are homogenously distributed throughout both tips, suggesting that no nanoscale structures (beyond those revealed by EBSD) have been subsampled by the APT lift out.

Th and Pb can be identified in the mass-to-charge spectrum for each dataset, with $^{232}Th^{++}$ forming a discrete peak at 116 Da and $^{208}Pb^{++}$ a peak at 104 Da (**Figure 5**). Peaks from singly charged or compound ions (e.g. ThO or ThO_2) could not be observed in either mass-to-charge spectrum. Th and Pb are distributed homogenously within both microtips, further supporting the lack of internal structure inferred from trace element distribution. Calculating the $^{208}Pb/^{232}Th$ ratio for microtip #01665 (subsampled from the patchy domain) yields a Pb-Th age of 2175 ± 143 (1σ) Ma, whereas microtip #01667 (sampled from the polysynthetically twinned domain) yields a Pb-Th age of 4328 ± 309 (1σ) Ma. Although ^{206}Pb and ^{207}Pb could not be confidently measured above background in younger microtip #01665, a calculated $^{207}Pb/^{206}Pb$ age of 4559 ± 396 (1σ) Ma in older microtip #01667 falls within uncertainty of the measured Pb-Th age. ^{238}U could not be confidently identified or quantified from the spectra in either dataset.

4. Discussion

4.1 Nanostructural characteristics of lunar baddeleyite

Baddeleyite in lunar meteorite NWA3163 exhibit a subset of the nano-scale features observed through EBSD analyses of baddeleyite from other shock metamorphic settings

(White et al., 2018) whereas the APT results differ (White, et al., 2017a). EBSD analysis reveals orthogonally-related crystallographic domains that result in an apparent overprinting of a polysynthetically twinned domain. Orthogonally related crosses defined by orientation data have been used to indicate partial to complete reversion from a high symmetry ZrO_2 polymorph (Cayron et al., 2010; Timms et al., 2017; White et al., 2018), though these relationships are incomplete in two of the grains (e.g. **Figure 3**) and absent in the grain chosen for APT analysis (**Figure 4**). Regarding APT results, phase transitions within baddeleyite grains at the Sudbury impact site (White et al., 2018) have previously been associated with the genesis of ~15 nm Fe clusters (White et al., 2017a; White et al., 2017b), whereby the introduction of nanoscale defects during phase transition (to either a high pressure or temperature polymorph) allowed cation mobility across nanometre-scale distances. The absence of clusters within NWA3163 baddeleyite suggests that either; (1) such nanoscale defects were not generated during phase transition, (2) that incompatible elements were forced from the lattice entirely during the shock and annealing process, preventing the formation of clusters, or (3) that the grain did not undergo transition to and reversion from a high symmetry polymorph. The decoration of subgrain boundaries by incompatible trace elements seen at the Sudbury site (White et al. 2017a) are also absent in our lunar sample. Given the absence of distinctive orthogonally related crosses in EBSD pole figures, we suggest that the core, polysynthetically twinned domain of grain #12,112 has not undergone any transition to the high symmetry tetragonal, orthorhombic or cubic ZrO_2 structures, and given the distinct orientation and texture of the partial rim around the core domain (Figure 4) we suggest that this microstructural domain represents recrystallization during a thermal event. Combined with the absence of phase transition related features in APT analysis, we suggest that the grain has not undergone transformation to a high symmetry ZrO_2 polymorph.

4.2 Accurate age resolution of lunar evolution

4.2.1 Targeting nanometre scale reset Th-Pb reservoirs to date impact events

The youngest Th-Pb APT age reported here (2175 ± 143 Ma) derives from the rim domain of grain #12,112, and overlaps with Ar-Ar estimates of late metamorphism between 2.0 and 2.5 Ga (Hudgins et al., 2011). The measured age also correlates with a purported high flux in lunar impacts between 1.8 and 2.2 Ga (Fernandes et al., 2013). This overlap allows the interpretation that the patchy baddeleyite domain overprints a primary, polysynthetically twinned core, accurately recording the timing of a major shock metamorphism event at ~2.1

Ga. It is expected that this younger age could not be spatially isolated using SIMS analysis as a result of the sub-micrometre size of the age reservoirs, yielding homogenized data variably influenced by lead loss and a common Pb component inherited from surrounding phases. A similar correlation between the deformational state of the grain and the extent of impact induced Pb loss has also been observed within SIMS analysis of martian shergottite NWA 5298 (Moser et al., 2013; Darling et al., 2016), suggesting that baddeleyite may record accurate impact ages within nanoscale domains in a wide variety of planetary materials. However, nanoscale targeting of shock reset domains, such as the overprinting baddeleyite rim revealed here by EBSD, using APT is required to confidently generate the youngest possible impact age. This approach could be critical for accurately verifying an intense period of lunar bombardment at ~3.9 Ga (Kring and Cohen, 2002; Cohen et al., 2000), evidence of which is notably absent in the baddeleyite record of NWA 3163.

4.2.2 Extraction of ancient U-Th-Pb crystallization ages from complex lunar materials

Given the occurrence of baddeleyite as a late-stage accessory phase in a large suite of mafic achondritic meteorites (Herd et al. 2017), it is likely that the analysed baddeleyite population crystallized directly from the final Zr-enriched magma associated with an early mafic melt such as a global lunar magma ocean (i.e. Elrado et al. 2011) or a re-working of it due to remelting and crystallization (McLeod et al. 2016). This provides a new approach to dating the more primitive forms of lunar magmatism recorded by NWA 3163 despite extensive granularization of the sample. Although acquired from an uncharacterised baddeleyite grain, the most robust Pb-Pb SIMS age (4308 ± 19 Ma; 98% radiogenic Pb) overlaps with the Th-Pb APT age generated from the polysynthetically twinned primary domain of grain #12,112 (4328 ± 309 Ma). Given the correlation of these ages with the calculated Rb-Sr model age for the source of NWA 3163 (4340 ± 57 Ma; McLeod et al., 2016) we suggest that the U-Th-Pb systematics of certain nanometre-scale domains (or rarely, whole grains) of baddeleyite record a robust crystallization age for the primary mafic protolith (**Figure 6**). While age analysis of these domains using individual microtip specimen produces accurate ages, these dates are largely imprecise (± 13.1 to 14.3% 2σ) due to the inherent counting statistical uncertainties associated with small (< 1,000 ions) peaks in the APT mass-to-charge spectra. As such, generating a reliable age from these domains will require either supplementary, higher precision chronology (i.e. SIMS) or weighted average measurements of multiple microtip specimens (e.g. White et al., 2017b) until such a time as there are improvements to the sensitivity of APT (Saxey et al., 2018). Assuming an initial formation age for the Moon of 4.51 Ga (Barboni et al., 2017), our new U-Th-Pb baddeleyite age (correlated by both APT and SIMS analysis) suggests primary mafic magmatism was still actively ongoing ~210 million years after lunar formation. Given that the ages of ferroan anorthosite suite rocks have previously been incorporated into studies which evidence the presence of a global lunar magma ocean until ~4290 Ma (Borg et al., 1999), it appears that the crystallization age attained here through both APT and SIMS analysis of NWA 3163 baddeleyite provides further support for either a prolonged lunar magma ocean or, more likely based on previous studies (e.g. McLeod et al., 2016), a major remixing event at c. 4.3 Ga. This chronological evidence is otherwise opaque in such highly metamorphosed samples. Such efforts will augment ongoing work to date these earliest lunar processes using zircon geochronology (Nemchin et al., 2009; Crow et al., 2017), and aid in refining the timeline for the formation and evolution of the Moon.

5. Conclusions

Coupled EBSD, SIMS and APT analysis of micro-baddeleyite grains has allowed for targeted U-Th-Pb dating of nanoscale crystallization (~4.33 Ga) and impact (~2.18 Ga) age domains in granulitic lunar breccia NWA 3163. Nanostructural analysis of the baddeleyite population reveals an abundance of complex, sub-micrometre features which are unresolvable at the length scales of SIMS analysis alone. Targeted extraction of these domains using FIB-SEM techniques allows for atom probe analysis of isolated subdomains, allowing high accuracy, low precision resolution of chronological end members. This facilitates the improved interpretation of more precise U-Pb SIMS data even for structurally uncharacterised baddeleyite. For NWA 3163, this includes placing an empirical crystallization age on the mafic protolith of the sample which, until now, has not been directly measured by radiogenic isotope systematics. This approach to nanogeochronology holds great promise in extracting accurate ages for the formation of many lunar, asteroidal and martian lithologies otherwise overprinted by metamorphic and bombardment events. Notably, these younger events can also be accurately (but imprecisely) dated using current APT technology.

Acknowledgments

L.F.W. acknowledges a postdoctoral fellowship supported by Hatch Ltd. NSERC Discovery Grants awarded to D.E.M and K.T.T are gratefully acknowledged. The work was supported by Royal Society Research Grant RG160237 awarded to J.R.D and a Department of Museum Volunteers Acquisitions & Research Fund awarded to K.T.T. We thank Axel Schmitt and Kevin Chamberlain for assistance with collection of the SIMS data reported in this study. The ion microprobe facility at UCLA is partly supported by a grant from the Instrumentation and Facilities Program, Division of Earth Sciences, National Science Foundation. The authors acknowledge the facilities, scientific and technical assistance of the Canadian Centre for Electron Microscopy (CCEM) at McMaster University, a national facility supported by the Canada Foundation for Innovation under the Major Science Initiative program, NSERC and McMaster University.

References

Barboni, M., Boehnke, P., Keller, B., Kohl, I.E., Schoene, B., Young, E.D., and McKeegan, K.D., 2017, Early formation of the Moon 4.51 billion years ago: Science Advances, v. 3, p. e1602365.

Blum, T.B., Darling, J.R., Kelly, T.F., Larson, D.J., Moser, D.E., Perez-Huerta, A., Prosa, T.J., Reddy, S.M., Reinhard, D.A., Saxey, D.W., Ulfig, R.M., and Valley, J.W., 2018, Best Practises for Reporting Atom Probe Analysis of Geological Materials, *in* Moser, D.E., Corfu, F., Darling, J.R., Reddy, S.M., and Tait, K. eds., Microstructural Geochronology: Planetary Records Down to Atom Scale, Wiley & Sons, p. 369–373.

Borg, L.E., Connelly, J.N., Boyet, M., and Carlson, R.W., 2011, Chronological evidence that the Moon is either young or did not have a global magma ocean.: Nature, v. 477, p. 70–72, doi: 10.1038/nature10328.

Borg, L., Norman, M., Nyquist, L., Bogard, D., Snyder, G., Taylor, L., and Lindstrom, M., 1999, Isotopic studies of ferroan anorthosite 62236: A young lunar crustal rock from a light rare-earth-element-depleted source: Geochimica et Cosmochimica Acta, v. 63, p. 2679–2691.

Cavosie, A.J., Erickson, T.M., Timms, N.E., Reddy, S.M., Talavera, C., Montalvo, S.D., Pincus, M.R., Gibbon, R.J., and Moser, D., 2015, A terrestrial perspective on using ex situ shocked zircons to date lunar impacts: Geology, v. 43, p. 999–1002, doi: 10.1130/G37059.1.

Cayron, C., Douillard, T., Sibil, A., Fantozzi, G., and Sao-Jao, S., 2010, Reconstruction of the cubic and tetragonal oarent grains from electron backscatter diffraction maps of monoclinic zirconia: Journal of the American Ceramic Society, v. 93, p. 2541–2544, doi: 10.1111/j.1551-2916.2010.03894.x.

Cohen, B.A., Swindle, T.D., and Kring, D.A., 2000, Support for the lunar cataclysm hypothesis from lunar meteorite impact melt ages: Science, v. 290, p. 1754–1756, doi: 10.1126/science.290.5497.1754.

Crow, C.A., McKeegan, K.D., and Moser, D.E., 2017, Coordinated U-Pb geochronology, trace element, Ti-in-zircon thermometry and microstructural analysis of Apollo zircons: Geochimica et Cosmochimica Acta, v. 202, p. 264–284.

Darling, J.R., Moser, D.E., Barker, I.R., Tait, K.T., Chamberlain, K.R., Schmitt, A.K., and Hyde, B.C., 2016, Variable microstructural response of baddeleyite to shock metamorphism in young basaltic shergottite NWA 5298 and improved U–Pb dating of Solar System events: Earth and Planetary Science Letters, v. 444, p. 1–12, doi: 10.1016/j.epsl.2016.03.032.

Elrado, S.M., Draper, D.S., and Shearer Jr, C.K., 2011, Lunar Magma Ocean crystallization revisited: Bulk composition, early cumulate mineralogy, and the source regions of the highlands Mg-suite: Geochimica et Cosmochimica Acta, v. 75, p. 3024–3045.

Erickson, T.M., Timms, N.E., Kirkland, C.L., Tohver, E., Cavosie, A.J., Pearce, M.A., and Reddy, S.M., 2017, Shocked monazite chronometry: integrating microstructural and in situ isotopic age data for determining precise impact ages: Contributions to Mineralogy and Petrology, v. 172, p. 1–19, doi: 10.1007/s00410-017-1328-2.

Fernandes, V.A.S.M., Fritz, J., Weiss, B.P., Garrick-Bethell, I., and Shuster, D.L., 2013, The bombardment history of the Moon as recorded by ^{40}Ar-^{39}Ar chronology: Meteoritics & Planetary Science, v. 48, p. 241–269.

Fernandes, V.A., Irving, A.J., Kuehner, S.M., Gellissen, M., Korotev, R.L., and Bandfield, J.L., 2009, Petrology, Bulk Composition, Ar-Ar Age and IR Emission Spectrum of Lunar Granulite Northwest Africa 4881, *in* 40th Lunar and Planetary Science Conference, The Woodlands, Texas,.

Fritz, J., Wunnermann, K., Greshake, A., Fernandes, V.A.S.M., Boettger, U., and Hornemann, U., 2011, Shock pressure calibration for lunar plagioclase, *in* 42nd Lunar and Planetary Science Conference, p. 1196.

Heaman, L.M., and LeCheminant, A.N., 1993, Paragenesis and U-Pb systematics of baddeleyite (ZrO_2): Chemical Geology, v. 110, p. 95–126.

Herd, C.D.K., Moser, D.E., Tait, K., Darling, J.R., Shaulis, B.J., and McCoy, T.J., 2018, Crystallization of Baddeleyite in Basaltic Rocks from Mars, and Comparisons with the Earth, Moon and Vesta, *in* Moser, D.E., Corfu, F., Darling, J.R., Reddy, S.M., and Tait, K. eds., Microstructural Geochronology: Planetary Records Down to Atom Scale,

American Geophysical Union, p. 137–165.
Hudgins, J., Kelley, S.P., Korotev, R.L., and Spray, J.G., 2011, Mineralogy, geochemistry, and ^{40}Ar-^{39}Ar geochronology of lunar granulitic breccia Northwest Africa 3163 and paired stones: Comparisons with Apollo samples: Geochimica et Cosmochimica Acta, v. 75, p. 2865–2881.
Irving, A.J., Kuehner, S.M., Korotev, R.L., Rumble III, D., and Hupe, G.M., 2006, Mafic granulitic impactites NWA 3163: A unique meteorite from the deep luar crust, *in* 37th Lunar and Planetary Science Conference, Houston, Texas,.
Joy, K.H., and Arai, T., 2013, Lunar meteorites: new insights into the geological history of the Moon: Astronomy and Geophysics, v. 54, p. 4.28-4.32.
Kring, D.A., and Cohen, B., 2002, Cataclysmic bombardment throughout the inner solar system 3.9–4.0 Ga: Journal of Geophysical Research, v. 107, p. 5009, doi: 10.1029/2001JE001529.
McLeod, C.L., Brandon, A.D., Fernandes, V.A., Peslier, A.H., Fritz, J., Lapen, T., Shafer, J.T., Butcher, A.R., and Irving, A.J., 2016, Constraints on formation and evolution of the lunar crust from feldspathic granulitic breccias NWA 3163 and 4881: Geochimica et Cosmochimica Acta, v. 187, p. 350–374.
Moser, D.E., Chamberlain, K.R., Tait, K.T., Schmitt, A. K., Darling, J.R., Barker, I.R., and Hyde, B.C., 2013, Solving the Martian meteorite age conundrum using micro-baddeleyite and launch-generated zircon.: Nature, v. 499, p. 454–7, doi: 10.1038/nature12341.
Moser, D.E., Cupelli, C.L., Barker, I.R., Flowers, R.M., Bowman, J.R., Wooden, J., and Hart, J.R., 2011, New zircon shock phenomena and their use for dating and reconstruction of large impact structures revealed by electron nanobeam (EBSD, CL, EDS) and isotopic U–Pb and (U–Th)/He analysis of the Vredefort dome: Canadian Journal of Earth Sciences, v. 48, p. 117–139, doi: 10.1139/E11-011.
Nemchin, A., Timms, N., Pidgeon, R., Geisler, T., Reddy, S., and Meyer, C., 2009, Timing of crystallization of the lunar magma ocean constrained by the oldest zircon: Nature Geoscience, v. 2, p. 133–136.
Papapavlou, K., Darling, J.R., Moser, D.E., Barker, I.R., White, L.F., Lightfoot, P.C., Storey, C.D., and Dunlop, J., 2018, U–Pb isotopic dating of titanite microstructures: potential implications for the chronology and identification of large impact structures: Contributions to Mineralogy and Petrology, v. 173, p. 82, doi: 10.1007/s00410-018-1511-0.

Saxey, D.W., Moser, D.E., Piazolo, S., Reddy, S.M., and Valley, J.W., 2018, Atomic worlds: Current state and future of atom probe tomography in geoscience: Scripta Materialia, v. 148, p. 115–121.

Schmitt, A.K., Chamberlain, K.R., Swapp, S.M., and Harrison, T.M., 2010, In situ U-Pb dating of micro-baddeleyite by secondary ion mass spectrometry: Chemical Geology, v. 269, p. 386–395, doi: 10.1016/j.chemgeo.2009.10.013.

Smith, D.K., and Newkirk, W., 1965, The crystal structure of baddeleyite (monoclinic ZrO_2) and its relation to the polymorphism of ZrO_2: Acta Crystallographica, v. 18, p. 983–991, doi: 10.1107/S0365110X65002402.

Timms, N.E., Erickson, T.M., Zanetti, M.R., Pearce, M.A., Cayron, C., Cavosie, A.J., Reddy, S.M., Wittmann, A., and Carpenter, P.K., 2017, Cubic zirconia in >2370 °C impact melt records Earth's hottest crust: Earth and Planetary Science Letters, v. 477, p. 52–58, doi: 10.1016/j.epsl.2017.08.012.

White, L.F., Darling, J.R., Moser, D.E., Cayron, C., Barker, I., Dunlop, J., and Tait, K.T., 2018, Baddeleyite as a widespread and sensitive indicator of meteorite bombardment in planetary crusts: Geology, v. 46, p. 719–722, doi: 10.1130/G45008.1.

White, L.F., Darling, J.R., Moser, D.E., Reinhard, D.A., Dunlop, J., Larson, D.J., Lawrence, D., and Martin, I., 2017, Complex nanostructures in shocked, annealed and metamorphosed baddeleyite defined by atom probe tomography, *in* Moser, D., Corfu, F., Reddy, S., Darling, J., and Tait, K. eds., Microstructural Geochronology: Planetary Records Down to Atom Scale, Hoboken, NJ, John Wiley & Sons, Inc.

White, L.F., Darling, J.R., Moser, D.E., Reinhard, D.A., Prosa, T.J., Bullen, D., Olson, D., Larson, D.J., Lawrence, D., and Martin, I., 2017, Atomic scale age resolution of planetary events: Nature Communications, doi: 10.1038/ncomms15597.

Figure Captions

Figure 1: Hand sample photograph of NWA 3163. The highly brecciated nature of the sample is apparent at this scale (~15cm long), with large fractured anorthositic clasts occurring in a fine-grained matrix. The complex nature of this meteorite makes the generation and interpretation of robust age data a challenge (Photo credit: Brian Boyle, ROM).

Figure 2: Backscatter electron (BSE) imaging of baddeleyite (Bdl) grains in NWA 3163. Grains are commonly in association with ilmenite (Ilm), though a single baddeleyite occurs

in flow textured plagioclase (#2294). The sample is highly brecciated, consisting of maskelynite (diaplectic glass of plagioclase composition) and pyroxene clasts within a fine-grained matrix.

Figure 3: Backscatter electron (BSE) and electron backscatter diffraction (EBSD) data for baddeleyite grains #5135 (**A, B**), #10350 (**C, D**) and #2294 (**E, F**). For all grains, inverse pole figure (IPF) colouring relative to the z-axis correlates with coloured pixels in presented <001> pole figure diagrams. All datasets contain tight groups of orthogonally related orientations, while a small amount of crystal plastic deformation (< 10°) can be seen in larger baddeleyite domains (i.e. red data in grain #5135, pink data in grain #10350).

Figure 4: Backscatter electron (BSE) images show the mineralogical setting of target baddeleyite (bdl) grain #12,112, which is comparable to all analysed grains, the euhedral morphology of the grain, and the relationship with the associated ilmenite (Ilm) grain (**A**). During FIB extraction of the grain for atom probe analysis (following cross sectional line C-C'), a perpendicular BSE image of the grain was captured, allowing better visualisation of the baddeleyite – ilmenite grain boundary in 3D (**B**). Band contrast imaging (**C**) reveals the highly variable crystallinity of the grain, with regions of poorly diffracting ZrO_2 occurring as discrete bands and domains throughout the grain, parallel to twin and grain boundaries. Phase mapping of both ilmenite and baddeleyite confirms the association of the two phases (**D**). Two discrete microstructural domains in inverse pole figure (IPF, z-axis) colouring of the baddeleyite dataset (**E**), comprised of a preserved core region with polysynthetic twinning, and an overprinting rim. The grey star represents the location of microtip specimen #01665 within the rim, while the white star highlights tip #01667 within the twinned core. Ilmenite retains undeformed polysynthetic twins. Indexed baddeleyite yields clusters of orthogonally related crystallographic orientations in all pole figures (i.e. <001>, **F**). EBSD data was collected at 75nm step size.

Figure 5: Full mass-to-charge spectra and mass-to-charge peaks for $^{232}Th^{++}$ (116 Da) and $^{208}Pb^{++}$ (104 Da) as isolated by atom probe tomography in microtip specimen #01665. All cation species, including Th and Pb, are predominately homogenously distributed throughout both analysed microtips; #01665 (baddeleyite rim, grey star) and #01667 (baddeleyite core, white star). Of note, the decoupling of Th and Pb observed in tip #1665 (grey star) does not

appear to affect the measured Th/Pb age, with the exclusion of the domain yielding an age within uncertainty of the whole tip age (2350 Ma).

Figure 6: SIMS $^{207}Pb/^{206}Pb$ and APT $^{208}Pb/^{232}Th$ ages for NWA 3163**.** Error bars represent 1σ uncertainties. These results reveal two discrete U-Th-Pb age reservoirs in baddeleyite, which can be correlated with the crystallization age of the rock (~4.3 Ga, as defined by published Rb-Sr age models (McLeod et al., 2016)) and the last known impact event to affect the sample (~1.95 Ga, defined by Ar-Ar dating (McLeod et al., 2016)). SIMS analysis further supports a 4308 ± 38 Ma crystallization age, yielding a concordant U-Pb age (2 s.e. uncertainty) from an uncharacterised grain. No evidence of a ~3.4 Ga granularization event, as determined by published Ar-Ar data (Hudgins et al., 2011; McLeod et al., 2016) was found in the chronological record of baddeleyite. By correlating with EBSD analysis of the grain (Figure 4) we show that the crystallographic domain preserving igneous polysynthetic twinning retains a ~4.3 Ga Th-Pb age, while the metamorphic rim records a younger ~2.1 Ga age. Isolated dating of these nanometre scale domains can only be achieved using APT.

Figure 1

Figure 2

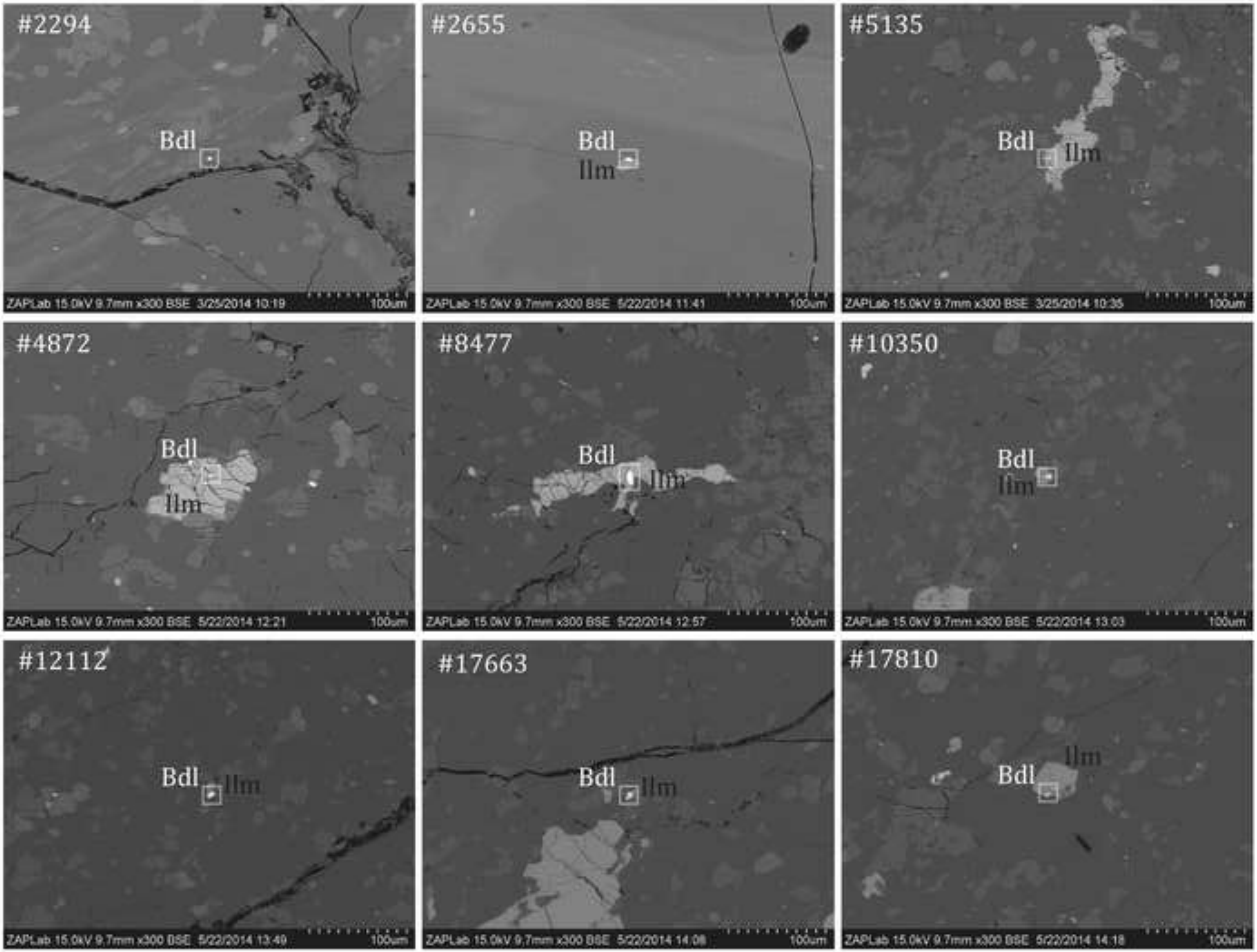
#2294
Bdl
ZAPLab 15.0kV 9.7mm x300 BSE 3/25/2014 10:19
100um
#2655
Bdl
Ilm
ZAPLab 15.0kV 9.7mm x300 BSE 5/22/2014 11:41
100um
#5135
Bdl
Ilm
ZAPLab 15.0kV 9.7mm x300 BSE 3/25/2014 10:35
100um
#4872
Bdl
Ilm
ZAPLab 15.0kV 9.7mm x300 BSE 5/22/2014 12:21
100um
#8477
Bdl
Ilm
ZAPLab 15.0kV 9.7mm x300 BSE 5/22/2014 12:57
100um
#10350
Bdl
Ilm
ZAPLab 15.0kV 9.7mm x300 BSE 5/22/2014 13:03
100um
#12112
Bdl
Ilm
ZAPLab 15.0kV 9.7mm x300 BSE 5/22/2014 13:49
100um
#17663
Bdl
Ilm
ZAPLab 15.0kV 9.7mm x300 BSE 5/22/2014 14:08
100um
#17810
Ilm
Bdl
ZAPLab 15.0kV 9.7mm x300 BSE 5/22/2014 14:18
100um

Figure 3

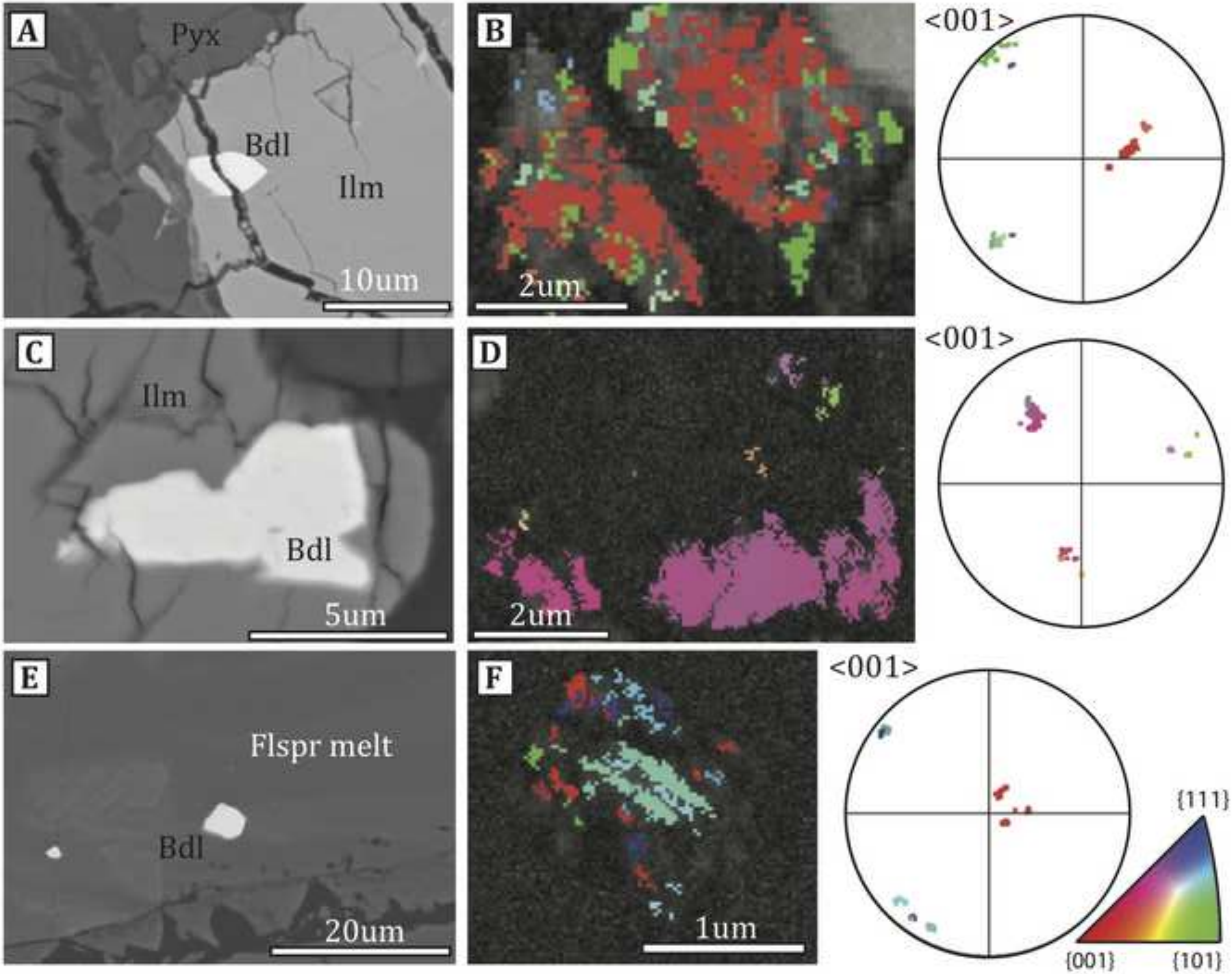

A
Pyx
Bdl
Ilm
10um
B
2um
<001>
C
Ilm
Bdl
5um
D
2um
<001>
E
Flspr melt
Bdl
20um
F
1um
<001>
{111}
{001}
{101}

Figure 4

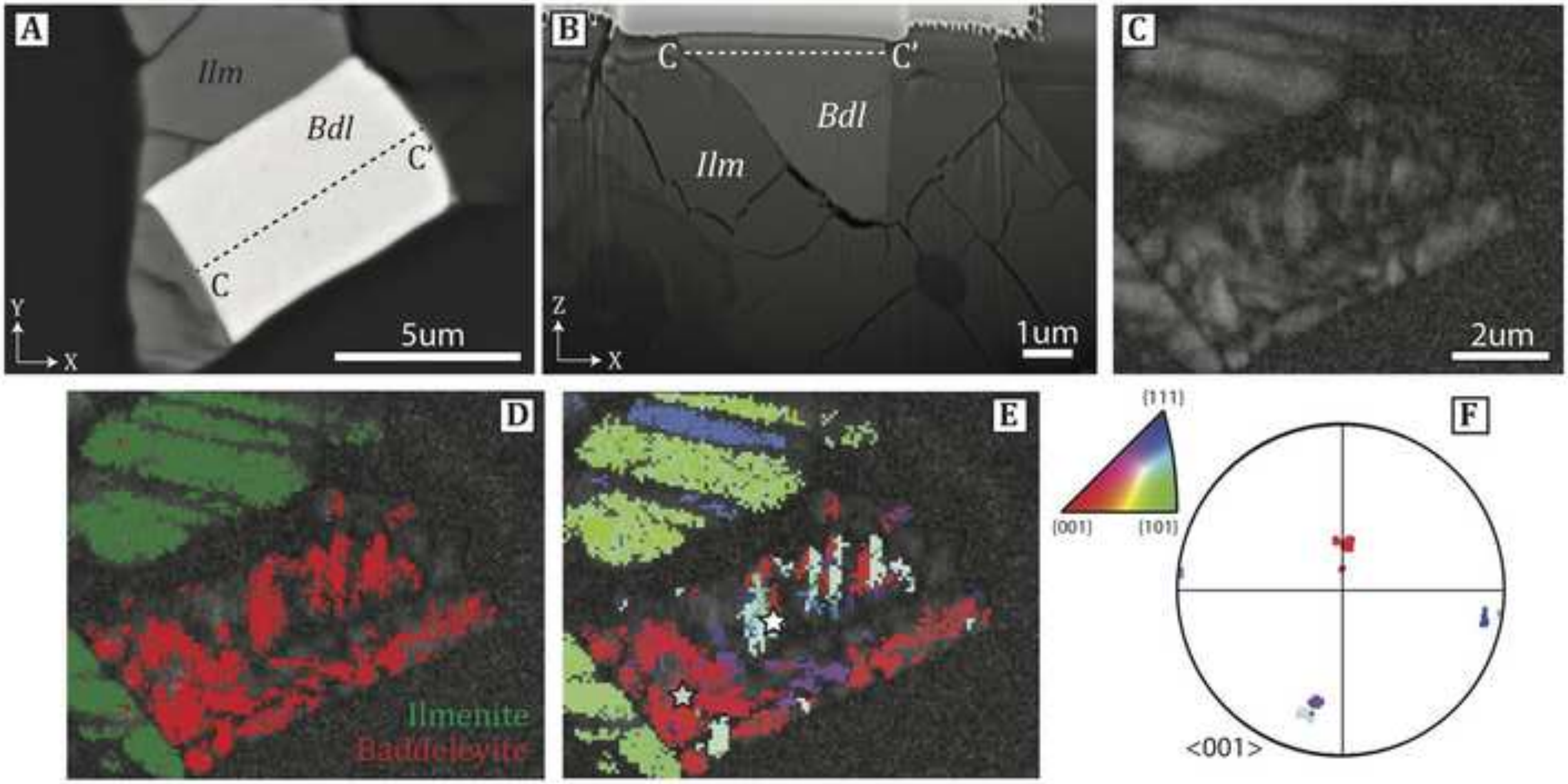
A
Ilm
Bdl
C'
C
Y
X
5um
B
C
C'
Bdl
Ilm
Z
X
1um
C
2um
D
Ilmenite
Baddeleyite
E
{111}
{001}
{101}
F
<001>

Figure 5

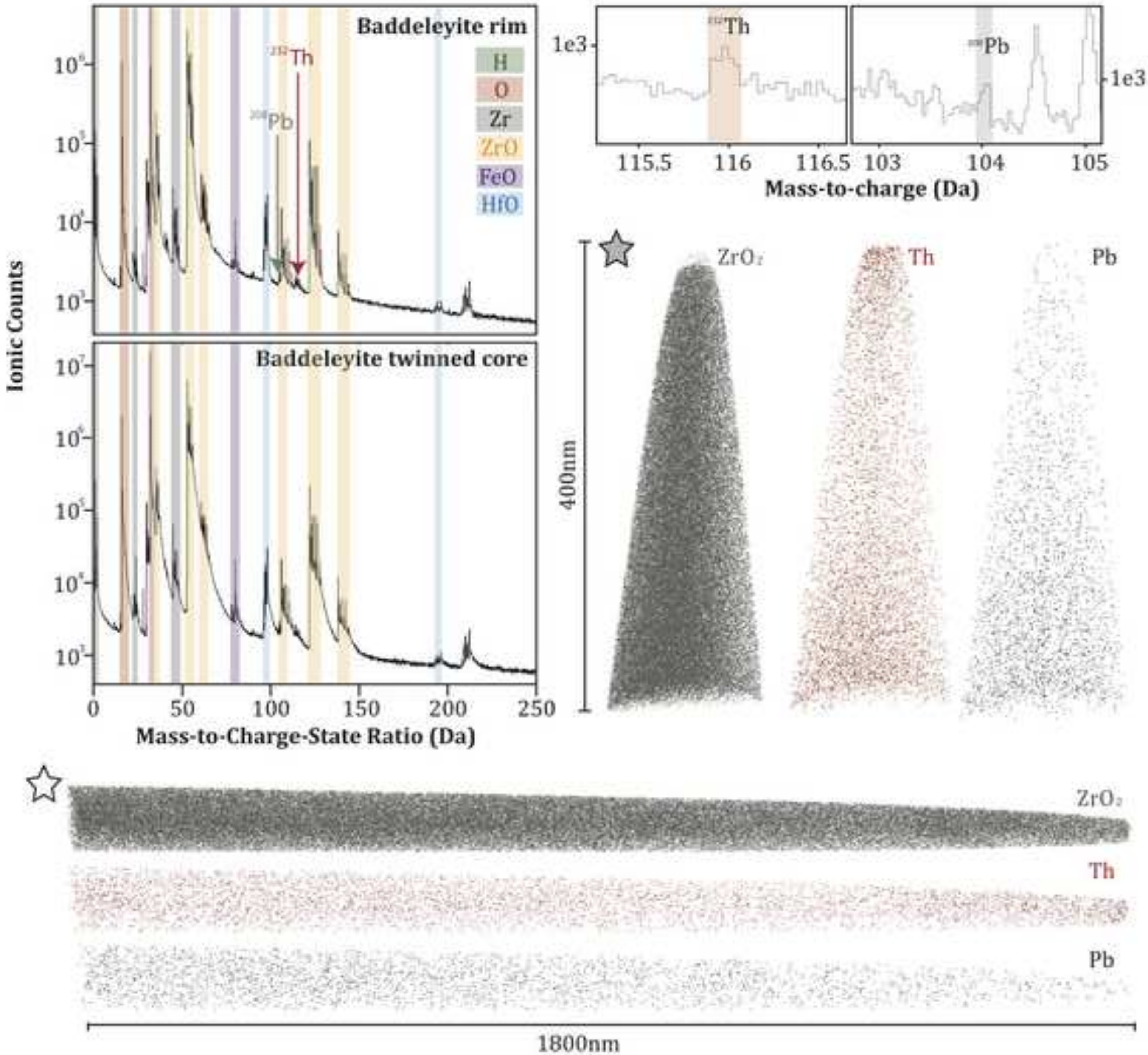

Baddeleyite rim
H
O
Zr
ZrO
FeO
HfO
232Th
208Pb
Baddeleyite twinned core
Ionic Counts
Mass-to-Charge-State Ratio (Da)
0
50
100
150
200
250
1e3
115.5
116
116.5
103
104
105
Mass-to-charge (Da)
ZrO2
Th
Pb
400nm
1800nm

Figure 6

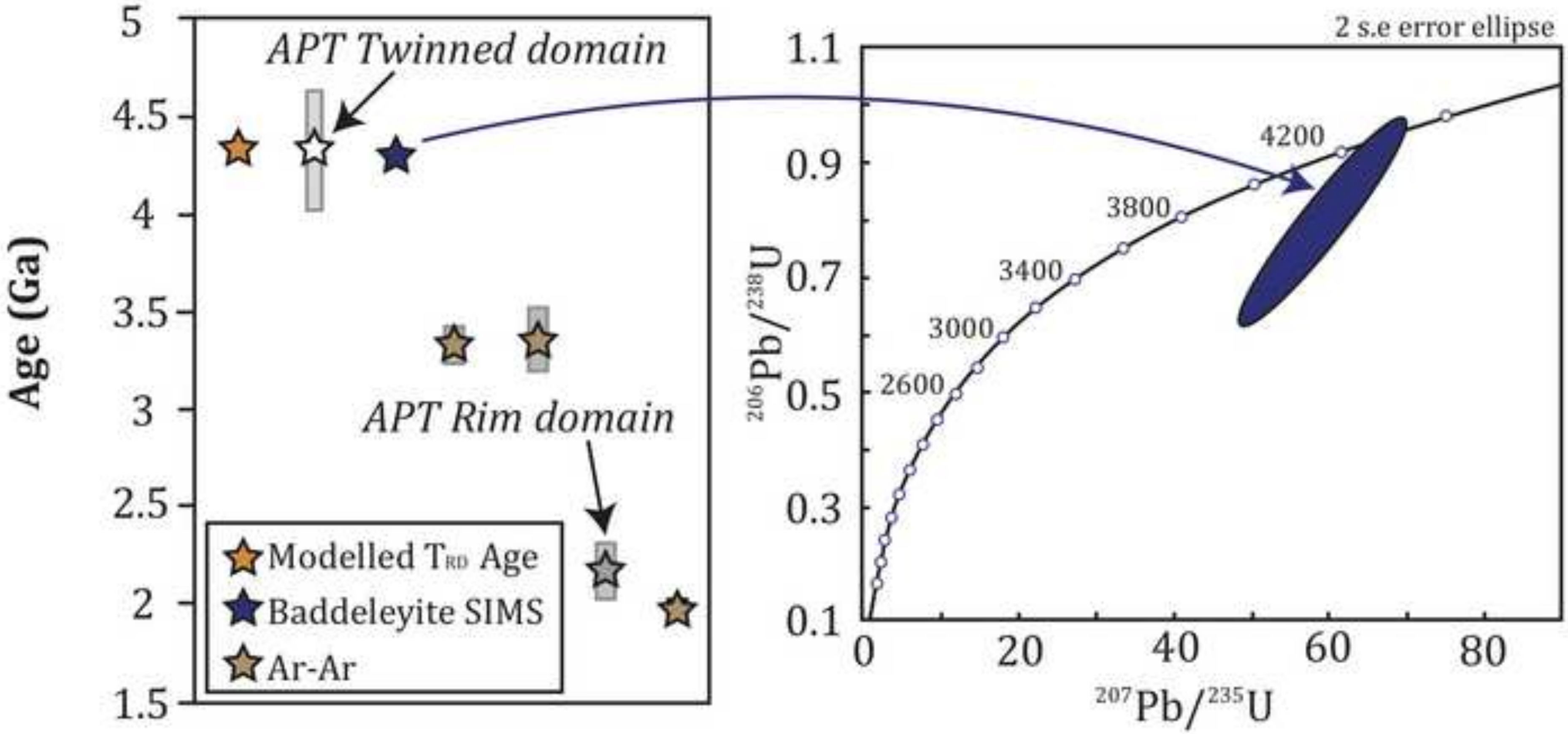

APT Twinned domain
APT Rim domain
Age (Ga)
5
4.5
4
3.5
3
2.5
2
1.5
Modelled TRD Age
Baddeleyite SIMS
Ar-Ar
2 s.e error ellipse
1.1
0.9
0.7
0.5
0.3
0.1
4200
3800
3400
3000
2600
206Pb/238U
0
20
40
60
80
207Pb/235U